23rd ABCM International Congress of Mechanical Engineering
December 6-11, 2015, Rio de Janeiro, RJ, Brazil

ANALYSIS AND DEVELOPMENT OF A PARALLEL 2 DOF MANIPULATOR

William Schroeder Cardozo
billi83@globo.com

Hans Ingo Weber
Pontifical Catholic University of Rio de Janeiro – PUC Rio, http://www.puc-rio.br/
hans@puc-rio.br

Abstract. *A parallel two-degree-of freedom manipulator designed for a variable orientation of a body in space is presented. The manipulator consists of one universal joint with the input axis fixed to the base and the output axis fixed to a moving platform. One possible application of this kind of device is on spacecrafts to orientate the rocket nozzle. Two linear servo hydraulic actuators are used in parallel to move the platform. On each fork of the universal joint an angular position sensor is mounted to measure the relative motion of the cross, instead of measuring the actuators displacement. First the kinematics of the manipulator is analyzed and a geometric description is given. Second, using Newton-Euler formulation, a dynamic analysis is done and the forces and torques acting on moving platform are obtained. After that, numerical simulations are performed using servo actuators forces as inputs while other simulations are done imposing the trajectory.*

Keywords: *Universal joint, Kinematics, Electrohydraulic Servosystem, Servoactuator, Angular Transducer*

1. INTRODUCTION

The most widespread method to orientate a rocket consists in controlling an aerodynamic device to generate moment about its center of mass. But, if a greater agility is required or if the vehicle moves in a low pressure atmosphere, the aerodynamic method is inadequate. In this case, thrust vector control (TVC) is used. The TVC deflects the propulsive vector from the center line of the rocket to produce moment about the center of mass. The deflection can be produced by tilting the nozzle assembly. In this case a gimbaled rocket nozzle assembly with two hydraulic actuators shifts the gimbal angles varying the direction of the force vector (Lazic and Ristanovic, 2006). A similar configuration is also used for underwater vehicles (Xin, *et al.*, 2013).The hydraulic actuator has been used to orientate the nozzle for a long time, but in recently years the utilization of an electromechanical actuator has grown (Li, *et al.*, 2012). In this work, an electrohydraulic system is used because it provides large forces with high load stiffness and high speed of response (Jelali and Kroll, 2003). It also has high power to weight ratio, good controllability and self lubrication property (Ghosh *et al.*, 2014).

In this paper a platform is fixed to the output shaft of a universal joint, as the nozzle assembly on TVC, while the input shaft is fixed to the base. Unlike constant velocity joints, like Rzeppa or Thomson coupling, the universal joint generates angular acceleration at the output axis in relation to the input axis (Watson, *et al.*, 2013). The consequence of this acceleration is analyzed in this work. Two linear hydraulic actuators are mounted in parallel between the platform and the base to control the two gimbal angles, thus forming a parallel manipulator (PM). During the last decades, PM has been a common research topic. Despite its more complex dynamics, it achieves more positioning accuracy and stiffness when compared to serial manipulator (Diáz-Rodriguez, *et al.*, 2013). In this work, the actuators are equal and its mounting points are symmetric, making the kinematics analysis simpler (Taghirad, 2013). There are two dynamical problems: direct dynamic and inverse dynamic. The direct dynamic problem simulates the response of the manipulator corresponding to a set of forces/torques applied at the actuators. The inverse dynamic problem searches for the forces/torques required to perform a desired trajectory (Tsai, 1999).

First the kinematics of the system is analyzed and a geometric description is given. Second, using Newton-Euler formulation an analysis of forces and torques acting on the moving platform is performed. With the kinematic and dynamic model, some numerical simulations are done based on the direct and inverse dynamic problems.

2. KINEMATICS

Fig. 1 shows the kinematics scheme of the parallel two degree of freedom platform (2dof) with a load. One shaft of the universal joint is fixed to a fixed base. The point B is the center of the fixed base and O is the center of the crosshead of the universal joint. A smaller universal joint connects the hydraulic actuators to the base and a ball joint connects it to the platform. The points C_{31} and C_{32} are the centers of actuators ball joints. C_{21} and C_{22} are the centers of actuators universal joint crossheads. P and L are the centers of mass of the moving platform and the load, respectively. C is the center of the top surface of the moving platform.

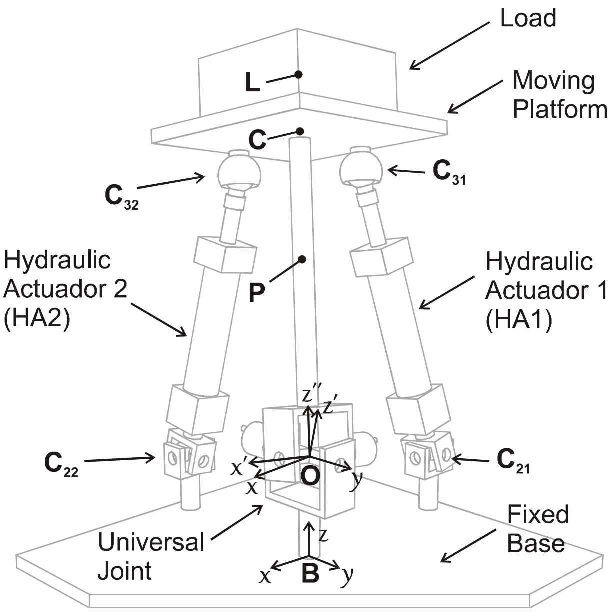

Figure 1. Kinematic scheme

Three references frames are defined, F fixed to the base, R attached to the main crosshead and S attached to the moving platform. The rotation between the frames are summarized by the following indication,

$$\underbrace{F}_{\substack{Base\\Fixed\\(x,y,z)}} \xrightarrow{\beta(y)} \underbrace{R}_{\substack{Main\\Crosshead\\(x',y,z')}} \xrightarrow{\propto(x')} \underbrace{S}_{\substack{Moving\\Platform\\(x',y'',z'')}}$$

β is the angle of rotation around the y-axis and α is around the x'-axis. Both angles are measured using angular transducers. The transformation (or rotation) matrix ${}^{F}\boldsymbol{T}^{R}$ leads from F to R,

$${}^{F}\boldsymbol{T}^{R} = \begin{bmatrix} cos\beta & 0 & sin\beta \\ 0 & 1 & 0 \\ -sin\beta & 0 & cos\beta \end{bmatrix}, \tag{1}$$

and ${}^{R}\boldsymbol{T}^{S}$ leads from R to S,

$${}^{R}T^{S} = \begin{bmatrix} 1 & 0 & 0 \\ 0 & cos\alpha & -sin\alpha \\ 0 & sin\alpha & cos\alpha \end{bmatrix}. \tag{2}$$

The angular velocity vector of the main crosshead using R or F coordinates is given by,

$${}_{F}^{R}\underline{\boldsymbol{\omega}}_{R} = {}_{F}^{F}\underline{\boldsymbol{\omega}}_{R} = \begin{bmatrix} 0 \\ \dot{\beta} \\ 0 \end{bmatrix}. \tag{3}$$

The vector of angular velocity related to the main crosshead of the moving platform, using R or S coordinates, is shown by,

$${}_{R}^{R}\underline{\boldsymbol{\omega}}_{S} = {}_{R}^{S}\underline{\boldsymbol{\omega}}_{S} = \begin{bmatrix} \dot{\alpha} \\ 0 \\ 0 \end{bmatrix}. \tag{4}$$

Hence, Eq.(5) gives the angular velocity of the moving platform using S coordinates,

$$ {}_{F}^{S}\underline{\boldsymbol{\omega}}_{S} = {}^{S}\boldsymbol{T}^{R}\, {}_{F}^{R}\underline{\boldsymbol{\omega}}_{R} + {}_{R}^{S}\underline{\boldsymbol{\omega}}_{S} \, . \tag{5} $$

The position of the center of mass of the platform using S coordinates is given by,

$$ {}_{O}^{S}\underline{\boldsymbol{r}}_{P} = \begin{bmatrix} 0 \\ 0 \\ l_P \end{bmatrix}. \tag{6} $$

The same position, using the fixed frame F is present by,

$$ {}_{O}^{F}\underline{\boldsymbol{r}}_{P} = {}^{F}\boldsymbol{T}^{S}\, {}_{O}^{S}\underline{\boldsymbol{r}}_{P} \, . \tag{7} $$

Equation (8) shows the linear velocity of the center of mass of the moving platform,

$$ {}^{S}\underline{\boldsymbol{v}}_{P} = {}_{F}^{S}\widetilde{\boldsymbol{\omega}}_{S}\, {}_{O}^{S}\underline{\boldsymbol{r}}_{P} \, , \ where\, {}_{F}^{S}\widetilde{\boldsymbol{\omega}}_{S} = \begin{bmatrix} 0 & -\omega_z & \omega_y \\ \omega_z & 0 & -\omega_x \\ -\omega_y & \omega_x & 0 \end{bmatrix}. \tag{8} $$

Changing the letters from P to L in the Eqs.(6-8), the kinematics of the load is obtained. The length of the hydraulic actuator 1 (HA1) is given by Eq.(9), where ${}_{C_{21}}^{F}\underline{\boldsymbol{r}}_{C_{31}}$ is a vector starting at the point C_{21} and finishing at C_{31},

$$ d_1 = \left| {}_{C_{21}}^{F}\underline{\boldsymbol{r}}_{C_{31}} \right|, \tag{9} $$

and the length of the hydraulic actuator 2 (HA2) is given by Eq.(10), where ${}_{C_{22}}^{F}\underline{\boldsymbol{r}}_{C_{32}}$ is a vector starting at the point C_{22} and finishing at C_{32},

$$ d_2 = \left| {}_{C_{22}}^{F}\underline{\boldsymbol{r}}_{C_{32}} \right|. \tag{10} $$

3. DYNAMICS

Due to symmetries of the moving platform, the inertia matrix about its center of mass is given by,

$$ {}^{S}\boldsymbol{I}_{P} = \begin{bmatrix} I_{1P} & 0 & 0 \\ 0 & I_{1P} & 0 \\ 0 & 0 & I_{3P} \end{bmatrix}. \tag{11} $$

The inertia matrix of the load about its center of mass is also considered principal,

$$ {}^{S}\boldsymbol{I}_{L} = \begin{bmatrix} I_{1L} & 0 & 0 \\ 0 & I_{1L} & 0 \\ 0 & 0 & I_{3L} \end{bmatrix}. \tag{12} $$

The vector of angular momentum of the moving platform using S frame about its center of gravity is introduced by,

$$ {}^{S}\underline{\boldsymbol{H}}_{P} = {}^{S}\boldsymbol{I}_{P}\, {}_{F}^{S}\underline{\boldsymbol{\omega}}_{S} \, . \tag{13} $$

The linear momentum vector of the platform is present by Eq.(14) using S frame,

$$ {}^{S}\underline{\boldsymbol{G}}_{P} = m_P\, {}^{S}\underline{\boldsymbol{v}}_{P} \, . \tag{14} $$

Changing the letters from P to L in the Eqs. (13-14), the linear and angular momentum of the load are obtained. Equation (15) shows the angular momentum of the system composed by the moving platform with the embarked load, about the center of the main crosshead, which is a fixed point, using S frame(Weber, 2015),

$$ {}^{S}\underline{\boldsymbol{H}}_{O} = {}^{S}\underline{\boldsymbol{H}}_{P} + {}_{O}^{S}\tilde{\boldsymbol{r}}_{P}\, {}^{S}\underline{\boldsymbol{G}}_{P} + {}^{S}\underline{\boldsymbol{H}}_{L} + {}_{O}^{S}\tilde{\boldsymbol{r}}_{L}\, {}^{S}\underline{\boldsymbol{G}}_{L} \, . \tag{15} $$

Using Euler's Law Eq.(16) gives the moment ${}^{S}\underline{\boldsymbol{M}}_{O}$ acting on the platform about the fixed point O using S frame,

$$ {}^{S}\underline{\boldsymbol{M}}_{O} = {}^{S}\dot{\underline{\boldsymbol{H}}}_{O} + {}^{S}_{F}\tilde{\boldsymbol{\omega}}_{S}\ {}^{S}\underline{\boldsymbol{H}}_{O}. \tag{16} $$

This moment is generated by the force vectors of hydraulics actuators $\underline{\boldsymbol{F}}_{a_1}$ and $\underline{\boldsymbol{F}}_{a_2}$, by gravity force $(m_P + m_L)\underline{\boldsymbol{g}}$ and by the reaction at the main crosshead $\underline{\boldsymbol{M}}_J$. The mass of the main crosshead is neglected. Equation (17) shows the moment of forces, using S frame,

$$ {}^{S}\underline{\boldsymbol{M}}_{O} = {}^{S}\boldsymbol{T}^{F}\left(\left(m_P\,{}^{F}_{O}\tilde{\boldsymbol{r}}_{P} + m_L\,{}^{F}_{O}\tilde{\boldsymbol{r}}_{L}\right){}^{F}\underline{\boldsymbol{g}} + {}^{F}_{O}\tilde{\boldsymbol{r}}_{C_{31}}\,{}^{F}\underline{\boldsymbol{F}}_{a_1} + {}^{F}_{O}\tilde{\boldsymbol{r}}_{C_{32}}\,{}^{F}\underline{\boldsymbol{F}}_{a_2}\right) + {}^{S}\underline{\boldsymbol{M}}_{J}. \tag{17} $$

The reaction on the main crosshead with magnitude M_J is given by Eq.(18) using S frame,

$$ {}^{S}\underline{\boldsymbol{M}}_{J} = {}^{S}\boldsymbol{T}^{R}\ {}^{R}\underline{\boldsymbol{M}}_{J} = {}^{S}\boldsymbol{T}^{R}\begin{bmatrix}0\\0\\M_J\end{bmatrix} = \begin{bmatrix}0\\M_J\,sin\alpha\\M_J\,cos\alpha\end{bmatrix}. \tag{18} $$

The force of the HA1 is given by Eq.(19), where F_{a1} is the magnitude,

$$ {}^{F}\underline{\boldsymbol{F}}_{a_1} = \frac{{}^{F}_{C_{21}}\boldsymbol{r}_{C_{31}}}{\left|{}^{F}_{C_{21}}\boldsymbol{r}_{C_{31}}\right|}F_{a1}. \tag{19} $$

The force of the HA2 is given by Eq.(20), where F_{a2} is the magnitude,

$$ {}^{F}\underline{\boldsymbol{F}}_{a_2} = \frac{{}^{F}_{C_{22}}\boldsymbol{r}_{C_{32}}}{\left|{}^{F}_{C_{22}}\boldsymbol{r}_{C_{32}}\right|}F_{a2}. \tag{20} $$

The magnitudes of these both forces are considered as a sum of a constant component F_1 and F_2 and a viscous damping with b_a as coefficient. Equation (21) shows how F_{a1} is calculated,

$$ F_{a1} = F_1 + b_a\dot{d}_1, \tag{21} $$

and Eq. (22) gives how F_{a2} is calculated,

$$ F_{a2} = F_2 + b_a\dot{d}_2. \tag{22} $$

The gravity vector using the fixed frame is presented by the Eq.(23), where g is the magnitude,

$$ {}^{F}\underline{\boldsymbol{g}} = \begin{bmatrix}0\\0\\-g\end{bmatrix}. \tag{23} $$

Defining τ_1, τ_2, and τ_3 as torques on the system, they are given by,

$$ \begin{bmatrix}\tau_1\\\tau_2\\\tau_3\end{bmatrix} = {}^{S}\boldsymbol{T}^{F}\left(\left(m_L\,{}^{F}_{O}\tilde{\boldsymbol{r}}_{L} + m_P\,{}^{F}_{O}\tilde{\boldsymbol{r}}_{P}\right){}^{F}\underline{\boldsymbol{g}} + {}^{F}_{O}\tilde{\boldsymbol{r}}_{C_{31}}\,{}^{F}\underline{\boldsymbol{F}}_{a_1} + {}^{F}_{O}\tilde{\boldsymbol{r}}_{C_{32}}\,{}^{F}\underline{\boldsymbol{F}}_{a_2}\right). \tag{24} $$

Using Eq. (16) and Eq. (17), the angular acceleration $\ddot{\alpha}$ about the x'-axis is given by,

$$ \ddot{\alpha} = \frac{\tau_1 - (I_{1P} + l_P{}^2 m_P - I_{3P} + I_{1L} + l_L{}^2 m_L - I_{3L})\dot{\beta}^2}{I_{1P} + l_P{}^2 m_P + I_{1L} + l_L{}^2 m_L} \tag{25} $$

And the angular acceleration $\ddot{\beta}$ about the y-axis is given by,

$$ \ddot{\beta} = \frac{\tau_2 + \left(2(I_{1P} + l_P{}^2 m_P + I_{1L} + l_L{}^2 m_L) - I_{3P} - I_{3L}\right)sin\alpha\ \dot{\alpha}\dot{\beta} - \tau_3 tan\alpha}{(I_{1P} + l_P{}^2 m_P + I_{1L} + l_L{}^2 m_L)cos\alpha - (I_{3P} + I_{3L})\ sin\alpha\ tan\alpha} \tag{26} $$

4. SIMULATIONS

All the simulations are performed on MATLAB® software. First the actuators forces are given and trajectory of the moving platform is calculated using Eqs. (25) and (26), this being the direct dynamic (Tsai, 1999). Table 1 shows the parameters of this simulation.

Table 1.Direct Dynamic Simulation Parameters

Parameter	Value
l_P	$202.2 \cdot 10^{-3}\ m$
m_P	$2.195\ kg$
I_{1P}	$1.025 \cdot 10^{-1}\ kg\ m^2$
I_{3P}	$6.708 \cdot 10^{-1}\ kg\ m^2$
l_L	$260.9 \cdot 10^{-3}\ m$
m_L	$0.5\ kg$
I_{1L}	$4.1 \cdot 10^{-3}\ kg\ m^2$
I_{3L}	$6.5 \cdot 10^{-3}\ kg\ m^2$
F_1	$18N$
F_2	$15N$
b_a	$100\ Ns/m$
${}^F\underline{\boldsymbol{g}}$	$[0 \quad 0 \quad -9.81]^T m/s^2$
${}_0^S\underline{\boldsymbol{r}}_{C_{31}}$	$[-65 \quad 0 \quad 207.9]^T \cdot 10^{-3}\ m$
${}_0^F\underline{\boldsymbol{r}}_{C_{21}}$	$[-135 \quad 0 \quad -30]^T \cdot 10^{-3}\ m$
${}_0^S\underline{\boldsymbol{r}}_{C_{32}}$	$[0 \quad -65 \quad 207.9]^T \cdot 10^{-3}\ m$
${}_0^F\underline{\boldsymbol{r}}_{C_{22}}$	$[0 \quad -135 \quad -30]^T \cdot 10^{-3}\ m$

Figure (2) shows the trajectory of the point C for this set of parameters. The final position of the universal joint is presented too.

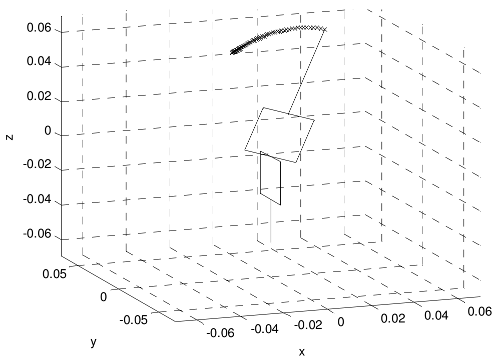

Figure 2.First trajectory of the point C

Figure 3 presents the gimbal angles α and β for this simulation, and the displacement of the actuators d_1 and d_2. The minimum length of the actuators is $0.198\ m$ and the maximum is $0.298\ m$, therefore its graphics are limited to those values.

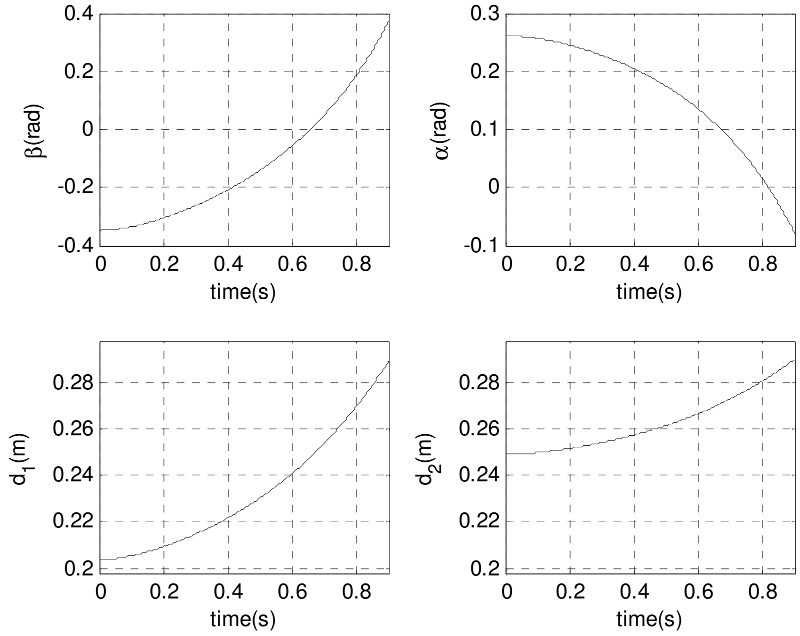

Figure 3. α, β, d_1 and d_2 vrs. time

Figure 4 shows the moment on z''-axis.

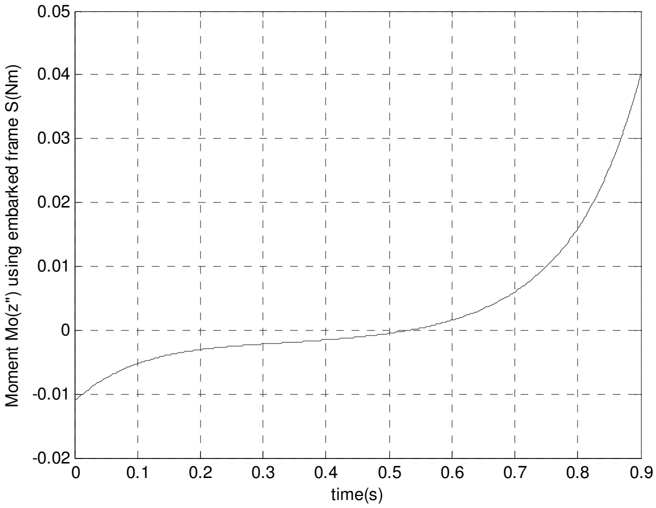

Figure 4.Moment on z''-axis for the first simulation.

Thereafter, a different kind of simulation is performed: the inverse dynamics (Tsai, 1999). Giving a trajectory the moments acting on the moving platform are calculated. This trajectory is defined using the articulation angle θ and the ϕ angle between the $-y$-axis andthe projection of z''-axis on the xy-plane. These angles are shown in Figure 5.

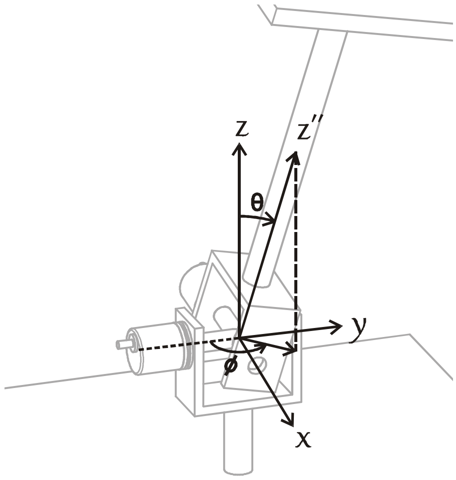

Figure 5. θ and ϕ definition

In the first simulation, the actuators are not able to perform wide articulation angles. Although, for this inverse dynamic simulation $\theta = 80°$, so the actuators of Fig. 1 cannot achieve this angle. Because of this, Eq. (16) is used to calculate the moment acting on the moving platform, instead of calculating the actuators force, as is typically done on inverse dynamic. This is done to analyze the performance of the platform in extreme angles. The angle ϕ changes with constant angular velocity$\dot{\phi} = 1\ rad/s$ from 0 to $2\pi\ rad$. In this case the parameters related to the moving platform and load are the same as in the previous simulation. Figure (6) shows the trajectory of the point C in this simulation.

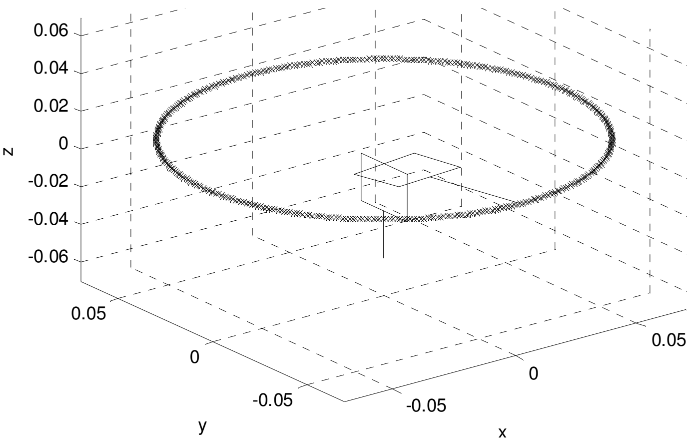

Figure 6. Second trajectory of the point C

Figure 7 shows the moment on z''-axis necessary to perform this movement using the embarked frame S. The moment on z''-axis is zero at $\phi = 0,\ \pi/2, \pi, 3\pi/2, 2\pi$. However, close to $\phi = 0, \pi, 2\pi$ it changes fast. The magnitude of the moment is much higher in this case because the articulation angle is much higher.

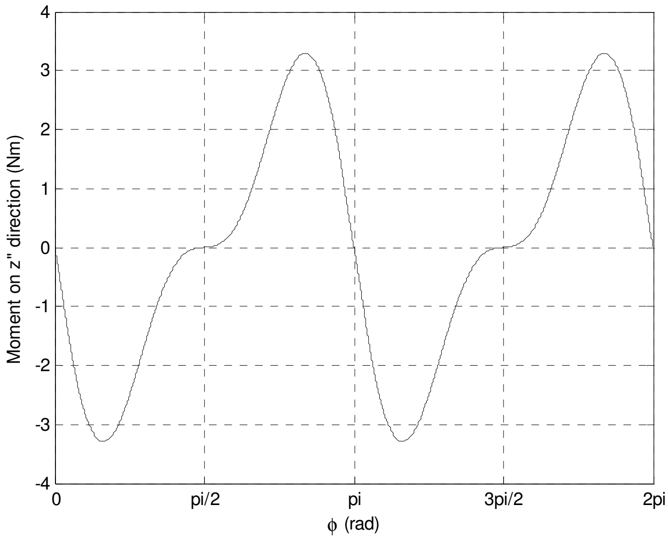

Figure 7.Moment on z''-axis for the second simulation

5. CONCLUSIONS

For the purpose of simulating the motion of the TVC, a mathematical model for the 2-dof platform was established. The kinematic and the dynamic analysis were presented. The analysis of the dynamic behavior of the moving platform was performed using two different simulations. In the first case, the actuators forces were used as input and the movement of the platform and the displacement of the actuators were calculated. The moment acting on the output axis of the universal joint was also calculated. In the second case, a given trajectory was used as input and the moment acting on the platform was calculated. The moment acting on the output axis of the universal joint was two orders of magnitude higher in the second simulation, mainly due to a much larger articulation angle.

A device is being built to validate the numerical results presented in this work. Furthermore, a control algorithm based on the inverse dynamics is being developed to control the platform motion.

6. REFERENCES

Lazic, D.V. andRistanovic, M.R., 2006. “Electrohydraulic thrust vector control of twin rocket engines with position feedback via angular transducers”. *Control Engineering Practice*, 15 (2007), 583–594.

Díaz-Rodriguez, M., Valera, A., Mata, V., Valles, M., 2013. “Model-Based Control of a 3-DOF Parallel RobotBased on Identified Relevant Parameters”. *IEEE/ASME Transactions on Mechatronics*, Vol. 18, No. 6, December 2013.

Ghosh, B.B., Sarkar, B.K., Saha, R., 2014. “Realtime performance analysis of different combinations of fuzzy–PIDand bias controllers for a two degree of freedom electrohydraulicparallel manipulator”, *Robotics and Computer-Integrated Manufacturing*, 34 (2015) 62–69.

Xin, B., Xiaohui, L., Zhaocun, S., Yuquan, Z., 2013.“A vectored water jet propulsion method for autonomous under water vehicles”, *Ocean Engineering*,74(2013)133–140.

Watson, I., Prusty, B.G., Olsen, J., 2013. “Conceptual design optimisation of a constant-velocity coupling”, *Mechanism and Machine Theory*, 68 (2013) 18–34.

Li, Y., Lu, H., Tian, S., Jiao, Z., Chen J.T., 2012. “Posture Control of Electromechanical-Actuator-Based Thrust Vector System for Aircraft Engine”, IEEE *Transactions On Industrial Electronics*, Vol. 59, No. 9, September 2012.

Jelali, M., Kroll, A., 2003. “Hydraulic Servo-systems Modelling, Identification and Control”, Springer, London, 2nd edition.

Tsai, L.W., 1999. “Robot Analysis The Mechanics of Serial and Parallel Manipulators”, John Wiley & Sons, New Jersey.

Taghirad, H.D., 2013. “Parallel Robots Mechanics and Control”, Taylor & Francis Group, Florida.

Weber, H.I.,, 2015. “Raciocinando Dinamica de Rotação”. Book under development, not published yet.

7. RESPONSIBILITY NOTICE